Numerical study of forced convection around heated horizontal triangular ducts

O. Zeitoun, M. E. Ali & A. Nuhait
King Saud University, Mechanical Engineering Department, Riyadh, Saudi Arabia

Abstract

Laminar forced convection heat transfer around horizontal triangular cross section ducts in air is investigated numerically. Equilateral triangle ducts of different cross section dimensions are investigated. The ducts are positioned such that the vertex of the triangle is facing the flow. The computational procedure is based on the finite element technique. Results are presented in the form of streamlines and temperature contour plots around the circumference of the ducts. Heat transfer data are generated and presented in terms of the average Nusselt number versus the Reynolds number, and the drag coefficient is also presented versus the Reynolds number and validated by comparing with that of a circular cylinder in cross flow. General correlations of Nusselt numbers in terms of wide ranges of the Reynolds number are obtained. Comprehensive discussion is also reported about the development of wakes downstream at the rear of the ducts.

Keywords: forced convection, heat transfer, laminar heat transfer, horizontal non-circular duct, triangular duct.

1 Introduction

Triangular ducts in cross flow have many engineering applications in the cooling of electronic components and heat exchangers. A survey of the literature shows that correlations for the overall averaged Nusselt numbers for forced convection heat transfer from circular and non-circular cylinders have been reported by different authors. Churchill and Bernstein [1] have reported a single comprehensive equation that cover the entire range of Reynolds numbers for a circular cylinder in cross flow for a wide range of Prandtl numbers as follows:

WIT Transactions on Engineering Sciences, Vol 68, © 2010 WIT Press
www.witpress.com, ISSN 1743-3533 (on-line)
doi:10.2495/HT100181

$$\overline{Nu}_D = 0.3 + \frac{0.62\,Re_D^{0.5}\,Pr^{1/3}}{\left[1+(0.4/Pr)^{2/3}\right]^{1/4}}\left[1+\left(\frac{Re_D}{282000}\right)^{5/8}\right]^{4/5} \quad (1)$$

Tables are also given for the empirical correlation to be used for noncircular cylinders in cross flow of gas by Eckert [2], Jakob [3], Gephardt [4] and Incropera and DeWitt [5]. Comprehensive archival correlations for average heat transfer coefficients for non-circular and circular cylinders and spheres in cross flow have been reported by Sparrow et al. [6]. Numerical simulation of two-dimensional flows over a circular cylinder using the immersed boundary method has been reported by Silva et al. [7]. An integral approach of the boundary layer analysis has been employed to investigate fluid flow and heat transfer from an infinite circular cylinder in cross flow by Khan et al. [8]. The effect of Reynolds and Prandtl numbers on heat transfer characteristics of an isothermal and isoflux sphere in the steady symmetric flow regime has been investigated by Dhole et al. [9]. Semi-circular tube in cross flow at different orientations has been studied by Nada et al. [10], cam shaped tube in cross flows has also been reported by Nouri-Borujerdi and Lavasani [11], and circular cylinder in cross flow to air and liquids has been investigated by Sanitjai and Goldstein [12]. Other shapes in cross flow such as square, diamond, elliptical, hexagonal, and rectangular cylinder have been investigated by Goldstein et al. [13], Yoo et al. [14], Ota et al. [15], Hilpert [16] and Igarashi [17] respectively. In all the cited papers, the triangular cylinders in cross flow have not been studied yet and there is no correlation available in the literature to report the average heat transfer coefficient from such cylinders which motivates the current study. The present investigation uses the computational fluid dynamics technique to report the flow and heat transfer characteristics around the triangular ducts (with an equilateral triangle cross section) in cross flow of air. Three isothermal surface triangular ducts are used in two different orientations to map out the different structures of streamlines and temperature contours as well as the velocity vectors around the ducts. Two overall correlations are obtained for a wide range of the Reynolds numbers to cover all ducts used in the two different orientations.

2 Mathematical formulation

The governing two-dimensional equations in a Cartesian coordinate system for unsteady, incompressible, laminar flow with negligible viscous dissipation and constant property fluids are given by:

$$\frac{\partial u}{\partial x} + \frac{\partial v}{\partial y} = 0 \quad (1)$$

$$\rho\,\frac{\partial u}{\partial \tau} + \rho\left(u\frac{\partial u}{\partial x} + v\frac{\partial u}{\partial y}\right) = -\frac{\partial p}{\partial x} + \mu\left(\frac{\partial^2 u}{\partial x^2} + \frac{\partial^2 u}{\partial y^2}\right) \quad (2)$$

$$\rho\,\frac{\partial v}{\partial \tau} + \rho\left(u\frac{\partial v}{\partial x} + v\frac{\partial v}{\partial y}\right) = -\frac{\partial p}{\partial y} + \mu\left(\frac{\partial^2 v}{\partial x^2} + \frac{\partial^2 v}{\partial y^2}\right) \quad (3)$$

$$\rho\ c_p \frac{\partial T}{\partial \tau} + \rho\ c_p \left(u \frac{\partial T}{\partial x} + v \frac{\partial T}{\partial y} \right) = k \left(\frac{\partial^2 T}{\partial x^2} + \frac{\partial^2 T}{\partial y^2} \right) \quad (4)$$

The boundary conditions for the present problem are specified as follows (Fig. 1):

- at inlet boundary at left: $u = u_\infty$, $T = T_\infty$ (5)
- on the top and bottom far field boundary: $u = u_\infty$, $T = T_\infty$ (6)
- on the surface of the body: $u = v = 0$, $T = T_w = \text{constant}$ (7)
- at exit boundary at right: $$\frac{\partial u}{\partial x} = \frac{\partial v}{\partial x} = \frac{\partial T}{\partial x} = 0 \quad (8)$$

The initial conditions are: at $\tau = 0$, $u = u_\infty$, $v = 0$, $T = T_\infty$

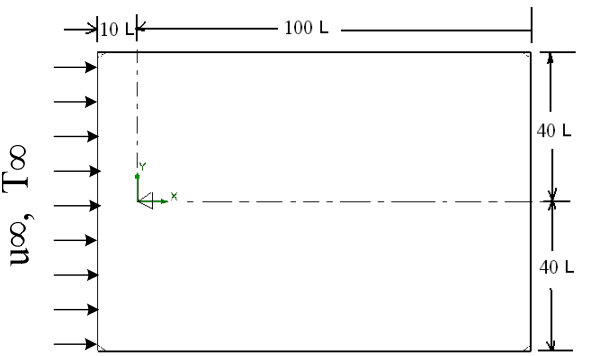

Figure 1: Dimensions of the solution domain of flow past triangular duct.

The solution domain is shown in Fig. 1. It should be noticed that the far field value at the bottom in the negative y-direction and in the x-direction are chosen far enough to satisfy the stated boundary conditions by Eqs. (6) and (8) respectively.

3 Numerical solution procedure

The present problem is solved using a finite element solver. The pressure field is calculated using the SIMPLE algorithm introduced by Patankar [18]. The hybrid-differencing scheme is used to differentiate the convective terms. The iterative solution is considered to have converged when the maximum of the residual across all nodes is less than 10^{-5} for continuity, velocities and temperature. The pressure-velocity coupling problem is solved by using the well-known SIMPLE method [18] where the velocity components are first solved using the assumed pressure. The pressure and velocity fields are then corrected based on the calculated values of pressure and velocities. This process is repeated until the residuals of all equations are negligible. A similar routine is used by Al-Sanea and Ali [19] and by Kiwan and Ali [20] to obtain the heat transfer and flow

fields near the extrusion slit of a continuously moving surface in plain and porous medium respectively, also by Zietoun and Ali [21] for natural convection over horizontal rectangular ducts in air. As shown in Fig. 2, four node quadrilateral cells were used in the current investigation. An automatic meshing technique was used to start the solution where about 10000 mesh systems were used in Fig. 2. Then, two-step automatic adaptive mesh technique was used to finish solution where these two steps has been ended by using about 50000 mesh system.

The current numerical model is validated by solving forced convection heat transfer around the horizontal isothermal circular cylinder in cross flow. The boundary conditions of the validation case are similar to the used ones in the

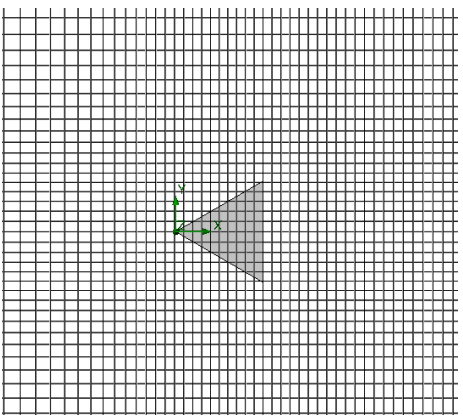

Figure 2: Meshing system of the solution domain showing the number of nodes (Focused mesh near the duct surface).

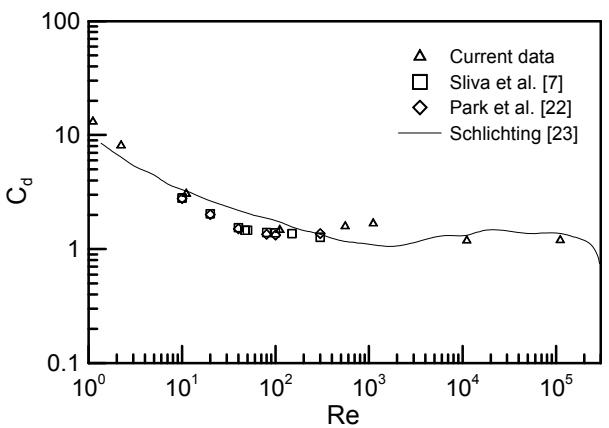

Figure 3: Drag coefficient for circular cylinders as a function of the Reynolds number showing comparison with the previous data in the literature.

current investigation, see Eqs. (5)–(8). Figure 3 represents this validation of total drag coefficient as a function of the Reynolds number, in the laminar range, compared with some of the numerical values available in the literature such as Silva et al. [7] and Park et al. [22]. The famous curve for drag coefficient of circular cylinders is also shown (Schlichting [23]) in Fig. 3 which shows good agreement with the current data. The current validation data of the average Nusselt numbers for forced convection over isothermal circular cylinder in cross flow are compared in Fig. 4 with the correlation of Churchill and Bernstein [1] which shows very good agreements. These comparisons make us confident about our computations and trust in the present results for horizontal triangular ducts in cross flow.

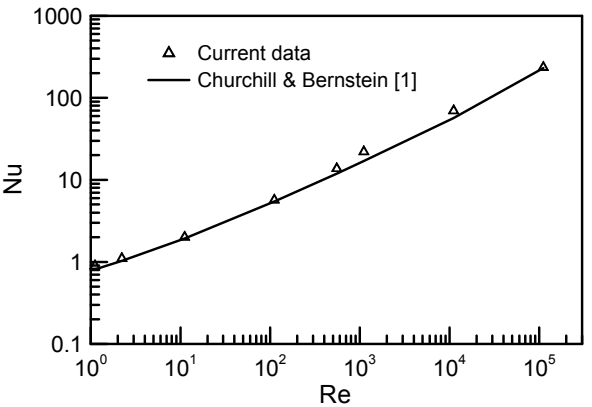

Figure 4: Comparison of the average Nusselt numbers for isothermal circular cylinder in cross flow with the correlation of Churchill and Bernstein [1].

4 Results and discussion

The current problem is solved for air and the run conditions are summarized in Table 1.

Several solutions are obtained for $1.3 \leq Re \leq 2 \times 10^5$ and for $Pr = 0.71$ corresponding to air flowing over the duct. Figure 5 illustrates the flow around a 0.025 m side length triangular duct at small Reynolds numbers, $Re = 1.38$, the stream flows smoothly past the body with no separation. Viscous effects are

Table 1: Run conditions.

Orientation	L, m	u_∞, m/s	T_w, K	T_∞, K
One vertex facing the flow	0.025	0.001 to 20	400	300
	0.05			
	0.1			

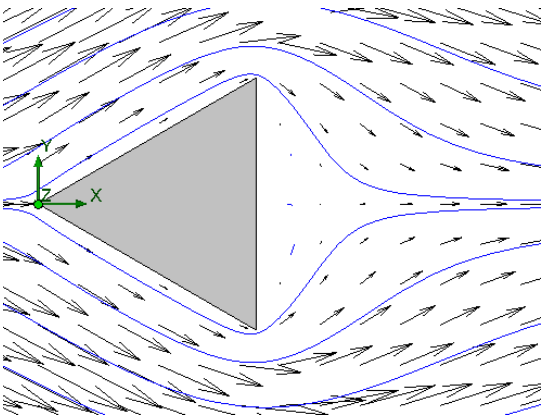

(a) Focused streamlines with velocity vectors around the body.

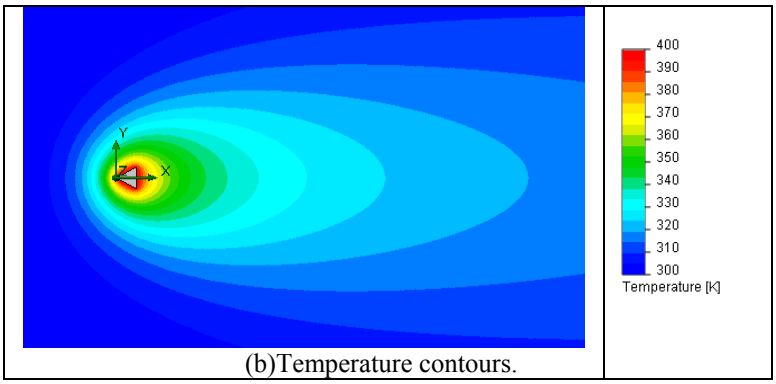

(b)Temperature contours.

Figure 5: Flow past a vertex facing triangle for Reynolds number = 1.38; (a) streamlines with velocity vectors and (b) temperature contours.

confined to a very thin boundary layer and the wake is very thin. The streamlines possess perfect fore-and-aft symmetry similar to creeping motion. The local velocity is everywhere retarded from its free stream value: there is no faster region such as occurs in potential flow. The velocity vectors show that the free stream fluid is brought to rest at the forward stagnation point, with an accompanying rise in pressure. From this point, the pressure decreases along the inclined sides of the duct and the boundary layer develops under the influence of favorable pressure gradient. Near the rear stagnation point the effective boundary layer thickness becomes large in this area.

The isothermal plot, Fig. 5(b), shows the thermal layers around the body that are symmetric about an axis that is parallel to the upstream flow and drawn through the vertex of the triangular duct. It can be seen that in this figure that the isothermal layers hug the surface of the duct and their thickness up stream is very thin compared to that downstream where they elongate and have elliptic

shape, since the heat diffuses downstream with the flow, until reaching the ambient temperature condition. Figure 6 illustrates the flow at Reynolds numbers, Re = 13.00, the stream flows smoothly past the inclined surfaces with separation points at the edges of the flat vertical side surface. Viscous effects are confined to a thin boundary layer along the inclined surfaces. The streamlines spread somewhat downstream.

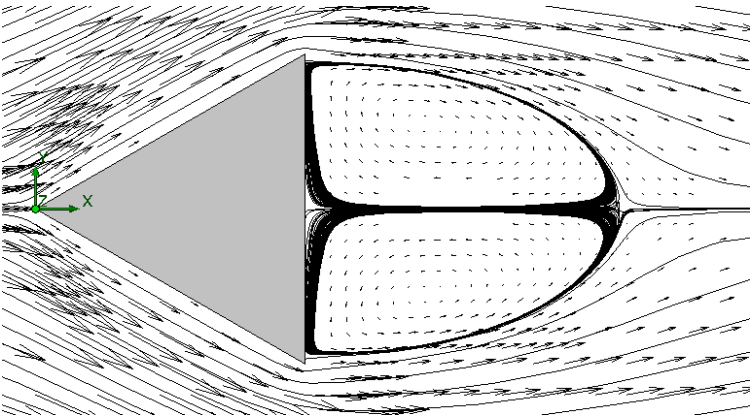

(a) Streamlines with velocity vectors.

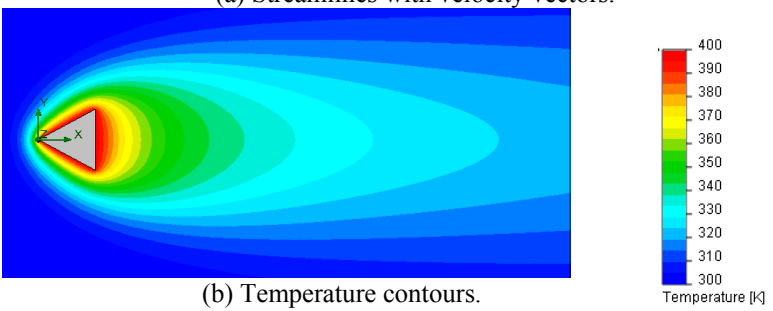

(b) Temperature contours.

Figure 6: Flow past a vertex facing triangle for Reynolds number = 13.00; (a) streamlines with velocity vectors and (b) temperature contours.

The local velocity is everywhere retarded from its free stream value: there is no faster region such as occurs in potential flow. Two standing small counter rotating eddies are formed as seen (Fig. 6(a)) and a second stagnation point downstream is observed where the flow is reattached. These symmetric vortices growing as Reynolds number increases up to a specific Re where they lose their symmetric and turned to be unsteady as will be seen in the next figures. It should also be noted that the flow is symmetric about an axis that is parallel to the upstream flow and drawn through the vertex of the triangular duct and the distance between the two stagnation points downstream of the body increases as Re increases. The isothermal layers shown in Fig. 6(b) are similar to those

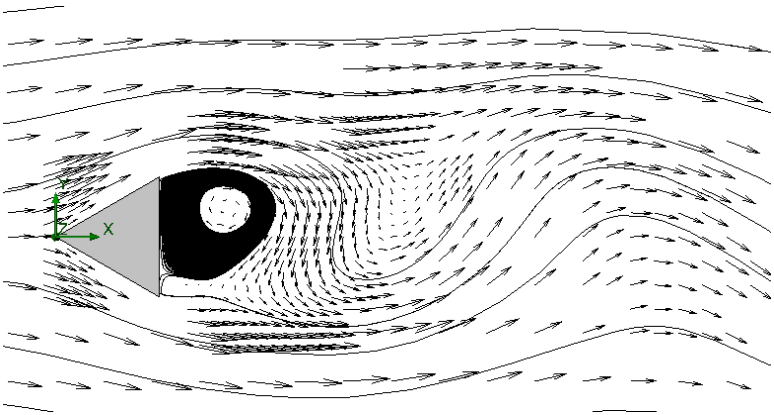

(a) Streamlines with velocity vectors.

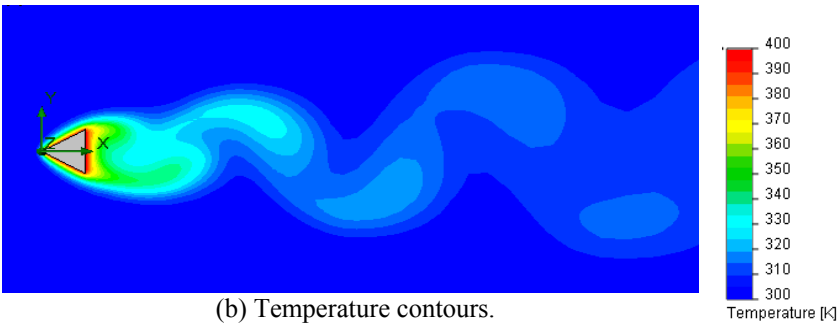

(b) Temperature contours.

Figure 7: Flow past a vertex facing triangle for Reynolds number = 69.4; (a) streamlines with velocity vectors and (b) temperature contours.

presented in Fig. 5(b) but they elongate more as Re increases. Figure 7 shows the flow at Reynolds numbers, Re = 69.40, the streamlines have lost symmetry about the centerline where the role of convective terms is distinct. Viscous effects are confined to a very thin boundary layer at the inclined surfaces with separation points near the end of these sides. The flow in the wake of the duct is unsteady due to the shedding of vortices from the rear portion of the duct as shown by the velocity vectors. This shedding causes the wake flow to be asymmetric about the duct axis. It is also clear that two unsteady eddies have formed behind the body in the wake flow. The velocities inside eddies are very small. The effect of eddies are clear on the isothermal layers in Fig. 7(b) where their loop thickness have reduced and lost symmetry about the centerline to adjust according to the flow features. This plot illustrates the formation of a thermal wake and vortex shedding process. As Reynolds number has continued to increase, separation has occurred at the rear of the body and more stronger unsteady eddies have formed behind the body. These unsteady eddies grow with Reynolds number. Viscous effects are confined to almost a zero boundary layer with striking alternating

vortices shed into the wake. The dimensionless drag coefficient is calculated by integrating pressure and shear stress x-components around the duct surface. Figure 8 shows the drag coefficient variation with Reynolds number when vertex of the duct facing the flow for three duct sizes. Inspection of Fig. 8 shows that at low Re O(1) the drag coefficient is high and the flow is symmetric and similar to creeping flow.

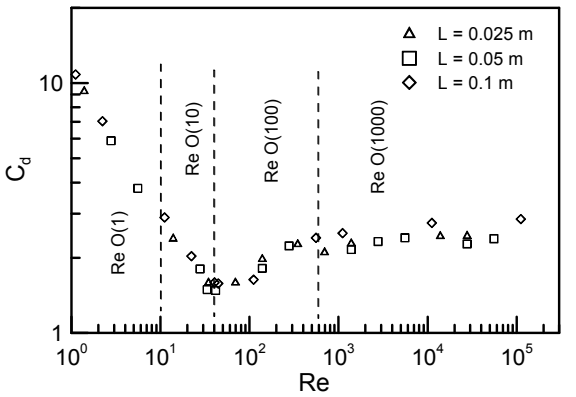

Figure 8: Drag coefficient of triangular ducts vertex facing the flow.

The drag coefficient decreases as Re increases up to O (10) where separation occurs but the flow still steady and symmetric about the centerline. However, as Re increases more O (100) the developed vortices turns to be unsteady and the drag coefficient increases until it reach almost constant value at high Re O (1000). This behavior of the drag coefficient is similar to the one developed over a circular cylinder before it reaches the drag crisis when the flow turns to be turbulent.

The total heat transfer from duct surfaces is calculated by integrating the local heat flux around the outer surface of the duct,

$$Q = \int_A q_W dA \quad (9) \qquad q_W = -k\left.\frac{\partial T}{\partial n}\right|_W \quad (10) \qquad Nu = \frac{hL}{k} \quad (11) \qquad h = \frac{Q}{(T_W - T_\infty)} \quad (12)$$

where the local heat flux is estimated by applying Fourier's law at the surface of the triangular ducts, where *n* is the normal direction to the surface. Nusselt number is defined and calculated using the triangular side length L as a characteristic length, where h is the average heat transfer coefficient around the surface. Figure 9 (a), (b) shows the variation of the average Nu numbers vs. Reynolds number for vertex of the duct facing the flow. Figure 9 (a) illustrates the data corresponding to the three different ducts used in this analysis where Nu increases as Re increases.

Figure 9 (b) shows the fitting curves to the data where the data is divided into three distinct regions corresponding to the regions defined by the drag coefficient (Fig. 8). The first correlation corresponding to a decreasing drag coefficient while the flow is symmetric is:

$$Nu = 0.856\ Re^{0.358},\ 0 < Re \leq 40 \quad (13)$$

with a correlation coefficient $R^2 = 0.987$. The second region represents the increase in the drag coefficient for separated asymmetry flow given by

$$Nu = 0.365\ Re^{0.596},\ 400 < Re \leq 700 \quad (14)$$

with a correlation coefficient $R^2 = 0.999$. The last region where the drag reaches almost a constant value corresponding to the following correlation

$$Nu = 0.633\ Re^{0.492},\ Re > 700 \quad (15)$$

with a correlation coefficient $R^2 = 0.994$. However, the three regions could be fitted using only one fitting correlation as following

$$Nu = 0.651\ Re^{0.486} \quad (16)$$

with a correlation coefficient $R^2 = 0.993$ where almost all the data lay between ± 15 % of error bands.

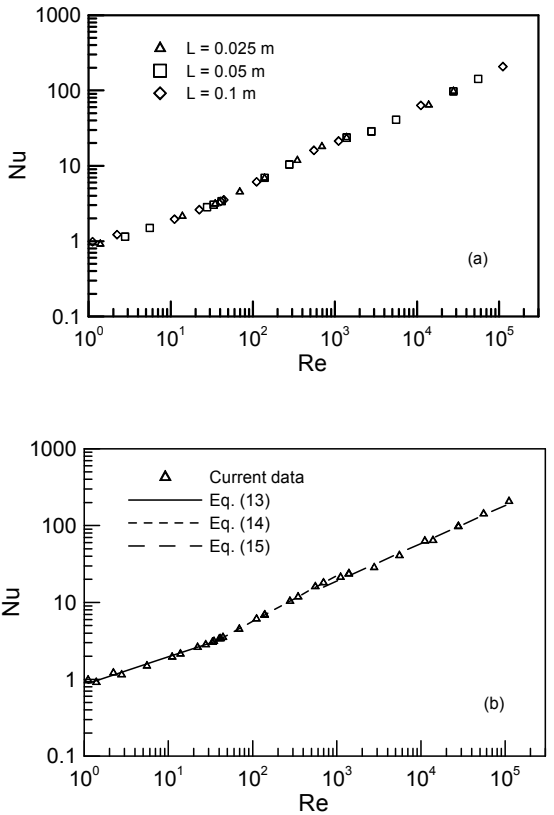

Figure 9: Numerical values of Nusselt numbers versus Reynolds numbers for vertex of the duct facing the flow; (a) symbols from all ducts and (b) all data showing different correlations for various distinct regions.

5 Conclusions

Forced convection from triangular cross section ducts has been investigated for wide ranges of Reynolds numbers. The average wall temperature of the circumference is computed and the average heat transfer coefficients are expressed in dimensionless form as Nusselt number. Velocity vectors and streamlines show that, for Re of order one the flow is symmetric around the duct with no separation points. For Re of order ten the; flow is still symmetric but with standing counter rotating vortices. However, as Re increases the flow is asymmetric with unsteady alternating vortices. Furthermore, drag coefficients are calculated and three distinct regions are obtained corresponding to Reynolds numbers which characterized by three correlations using the Nusselt numbers. Finally, general correlations of Nusselt numbers are obtained to represent the flow and heat transfer around the vertex facing duct.

Acknowledgements

This numerical investigation is supported by the Saudi Arabian Basic Industrial Company (SABIC) and the Research Center, College of Engineering at King Saud University under the project No. 35/428. This support is highly appreciated and acknowledged.

References

[1] Churchill, S. W. and Bernstein M., A correlating equation for forced convection from gases and liquids to a circular cylinder in cross flow. J. Heat Transfer, **99**, pp. 300–306, 1977.
[2] Eckert, E. R. G., *Introduction to the Transfer of Heat and Mass*, McGraw-Hill, New York, 1950.
[3] Jakob, M., *Heat Transfer*, vol. 1, John Wiley and Sons, Inc., New York, 1949.
[4] Gebhardt, B., *Heat Transfer*, McGraw-Hill, New York, 1961.
[5] Incropera, F. P., and DeWitt, D. P., *Introduction to Heat Transfer*, fifth ed., John Wiley and Sons Inc., New York, 2002.
[6] Sparrow, E. M., Abraham, J. P. and Tong, J. C. K., Archival correlations for average heat transfer coefficients for non-circular and circular cylinders and for spheres in cross-flow, Int. J. of Heat and Mass Transfer, **47**, pp. 5285–5296, 2004.
[7] Silva, A. L. F. L., Silveira-Neto, A. and Damasceno, J. J. R., Numerical simulation of two-dimensional flows over a circular cylinder using the immersed boundary method. J. of Computational Physics, **189**, pp. 351–370, 2003.
[8] Khan, W. A., Culham, J. R. and Yovanovich, M. M., Fluid flow around and heat transfer from an infinite circular cylinder. ASME, J. of Heat Transfer, **127**, pp. 785–790, 2005.

[9] Dhole, S. D., Chhabra, R. P. and Eswaran, V., A numerical study on the forced convection heat transfer from an isothermal and isoflux sphere in the steady symmetric flow regime. Int. J. of Heat and Mass Transfer, **49**, pp. 984–994, 2006.
[10] Nada, S. A., El-Batsh, H. and Moawed, M., Heat transfer and fluid flow around semi-circular tube in cross flow at different orientations. Heat and Mass Transfer, **43**, pp. 1157–1169, 2007.
[11] Nouri-Borujerdi, A. and Lavasani, A. M., Experimental study of forced convection heat transfer from a cam shaped tube in cross flows. Int. J. of Heat and Mass Transfer, **50**, pp. 2605–2611, 2007.
[12] Sanitjai, S. and Goldstein, R. J., Forced convection heat transfer from a circular cylinder in crossflow to air and liquids. Int. J. of Heat and Mass Transfer, **47**, pp. 4795–4805, 2004.
[13] Goldstein, R. J., Yoo, S. Y., and Chung, M. K., Convection mass transfer from a square cylinder and its base plate. Int. J. Heat and Mass Transfer, **33**, pp. 9–18, 1990.
[14] Yoo, S. Y., Goldstein, R. J., and Chung, M. K., Effects of angle of attack on mass transfer from a square cylinder and its base plate. Int. J. Heat Mass Transfer, **36**, pp. 371–381, 1993.
[15] Ota, T., Aida, S., Tsuruta, T. and Kaga, M., Forced convection heat transfer from an elliptic cylinder of axis ratio1: 2. Bull. JSME, **26**, pp. 262–267, 1983.
[16] Hilpert, R., Warmeabgabe von heheizten drahten und rohrem im iuftsstrom. Forsch. Geb. Ingenieurwes, **4**, pp. 215–224, 1933.
[17] Igarashi, T., Fluid flow and heat transfer around rectangular cylinders (the case of a width/height ratio of a section of o.33- 1.5). Int. J. Heat Mass Transfer, **30**, pp. 893–901, 1987.
[18] Patankar, S. V., *Numerical Heat Transfer and Fluid Flow*, Hemisphere, 1980.
[19] Al-Sanea, S. A. and Ali, M. E., The effect of extrusion slit on the flow and heat transfer characteristics from a continuously moving material with suction or injection. Int. J. Heat and Fluid Flow, **21**, No. 1, pp. 84–91, 2000.
[20] Kiwan, S. and Ali, M. E., Near-slit effects on the flow and heat transfer from a stretching plate in a porous medium. Numerical Heat Transfer, Part A, **54**, pp. 93–108, 2008.
[21] Zeitoun, O. and Ali, M., Numerical investigation of natural convection around isothermal horizontal rectangular ducts. Numerical Heat Transfer, Part A, **50**, pp. 189–204, 2006.
[22] Park, J., Kwon, K. and Choi, H., Numerical solutions of flow past a circular cylinder at Reynolds number up to 160. KSME Int. J., **12**, pp. 1200, 1998.
[23] Schlichting, H., *Boundary Layer Theory*, Seventh ed., McGraw-Hill, New York, 1979.